

## THE NEUTRINO MAGNETIC MOMENT PORTAL

V. BRDAR<sup>a,b</sup>, A. GRELJO<sup>c,d</sup>, **J. KOPP**<sup>c,e</sup> (speaker), T. OPFERKUCH<sup>c</sup>

<sup>a</sup> *Fermi National Accelerator Laboratory, Batavia, IL, 60510, USA*

<sup>b</sup> *Northwestern University, Department of Physics & Astronomy, Evanston, IL 60208, USA*

<sup>c</sup> *Theoretical Physics Department, CERN, 1211 Geneva, Switzerland*

<sup>d</sup> *Albert Einstein Center for Fundamental Physics, University of Bern, 3012 Bern, Switzerland*

<sup>e</sup> *PRISMA+ Cluster of Excellence, Johannes Gutenberg-Universität Mainz, 55099 Mainz, Germany*



We discuss neutrino magnetic moments as a way of constraining physics beyond the Standard Model. In fact, new physics at the TeV scale can easily generate observable neutrino magnetic moments, and there exists a multitude of ways of probing them. We highlight in particular direct dark matter detection experiments (which are sensitive to neutrino magnetic moments because of the predicted modifications to the solar neutrino scattering rate), stellar cooling, and cosmological constraints.

### 1 Neutrino Magnetic Moments as a Probe for “New Physics”

With the particle physics world abuzz about the intriguing anomaly observed in the magnetic moment of the muon, it is often forgotten that also the muon’s little siblings – the neutrinos – have magnetic moments. While unobservably tiny in Standard Model, these magnetic moments may be significantly enhanced in the presence of physics beyond the Standard Model, making them excellent indirect probes of “new physics”. In these proceedings, based largely on ref. [1], we discuss neutrino magnetic moments in the context of terrestrial, astrophysical, and cosmological probes, and we comment on intriguing model building aspects.

At the effective field theory (EFT) level, a neutrino magnetic moment is described by an operator of the form

$$\mathcal{L} \supset \frac{1}{2} \mu_\nu^{\alpha\beta} \bar{\nu}_L^\alpha \sigma^{\mu\nu} N_R^\beta F_{\mu\nu}, \quad (1)$$

where  $\mu_\nu^{\alpha\beta}$  is the magnetic moment (a constant of mass dimension  $-1$ ),  $\nu_L^\alpha$  and  $N_R^\beta$  are left-handed and right-handed neutrino fields, respectively,  $F^{\mu\nu}$  is the electromagnetic field strength tensor, and  $\alpha, \beta$  are flavor indices. The operator in eq. (1) is typically generated via loop diagrams such as the ones shown in fig. 1 as an example. Note in particular that because magnetic moment operators couple left-handed states to right-handed ones, they are sensitive to the mechanism

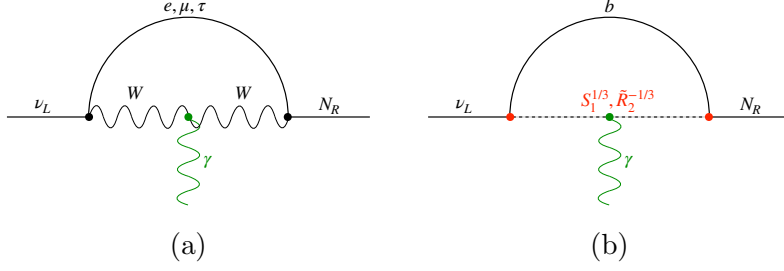


Figure 1 – Diagrams contributing to the neutrino magnetic moment (a) in the SM and (b) in a leptoquark model.

of neutrino mass generation. For Dirac neutrinos, the  $N_R$  are new states that are as light as the  $\nu_L$ . For Majorana neutrinos, the anti-particles of the  $\nu_L$  can play the role of the  $N_R$ ; in that case, the flavor-diagonal components of  $\mu_\nu^{\alpha\beta}$  vanish and only the off-diagonal ones (“transition magnetic moments”) are non-zero as can be verified with a bit of Dirac algebra. In both cases, the coupling of the right-handed states to the  $W$  – which is needed for the generation of  $\mu_\nu^{\alpha\beta}$  in the SM, see fig. 1 (a) – is suppressed by their mass, explaining the smallness of  $\mu_\nu^{\alpha\beta}$  in the SM [2–8].

This mass suppression is avoided in extensions of the SM such as the one shown in fig. 1 (b). In this example, leptoquarks with  $SU(3) \times SU(2) \times U(1)$  quantum numbers of  $(\bar{\mathbf{3}}, \mathbf{1}, 1/3)$  and  $(\mathbf{3}, \mathbf{2}, 1/6)$  are introduced. The former one, called  $S_1$ , could explain the  $R(D^{(*)})$  and muon  $g - 2$  anomalies (see refs. [1, 9–19] and section 4), while the second one is introduced in the context of the Voloshin mechanism [20] to avoid unacceptably large contributions to the neutrino mass matrix without tuning. It is intriguing that models of TeV-scale new physics that have been proposed for other reasons can naturally lead to sizeable neutrino magnetic moments. For instance, based on naive dimensional analysis, the diagram in fig. 1 (b) predicts  $\mu_\nu \sim e m_b / (16\pi^2 m_{LQ}^2) \sim 10^{-11} \mu_B$ , where  $m_{LQ} \sim \text{TeV}$  is the mass of the leptoquark,  $e$  is the electromagnetic gauge coupling,  $m_b$  is the bottom quark mass (responsible for the chirality flip in the diagrams), and  $\mu_B = e/(2m_e)$  is the Bohr magneton, the conventional unit for magnetic moments. As we will see in the following sections, such values of  $\mu_\nu$  are well within reach of current experiments, depending on the mass of the  $N_R$ .

## 2 Direct Detection of Neutrino Magnetic Moments

A particularly promising way of detecting neutrino magnetic moments is offered by detectors searching for dark matter scattering on nuclei and electrons. As is well known, solar neutrinos are an irreducible background to these searches [23–25]. Interestingly, for non-negligible  $\mu_\nu$ , the solar neutrino scattering rate is enhanced  $\propto 1/E_r$  at low recoil energies  $E_r$  due to the process being mediated by a massless photon. This makes dark matter detectors with their low recoil energy thresholds ideal tools to search for neutrino magnetic moments. This is illustrated in fig. 2, where we compare the expected electron recoil spectrum with and without neutrino magnetic moments to the data from Xenon1T [22] and Borexino [21] (see also refs. [24, 26, 27]). If the right-handed neutrino states are very light (blue line), we see a pronounced enhancement of the event rate at low recoil energies, relevant to Xenon1T and other dark matter detectors, while at higher energies, where dedicated solar neutrino experiments like Borexino are sensitive, the magnetic moment effect is negligible. For heavier right-handed neutrinos (red line), the scattering kinematics are modified such that the kinks in the spectrum (originating from the kinematic thresholds of the different components of the solar neutrino flux) are shifted. In this case, significant deviations from the Standard Model prediction are possible also at larger energies.

Translating these results into constraints, we see in fig. 3 that Xenon1T is currently the most sensitive terrestrial probe of neutrino magnetic moments for low right-handed neutrino

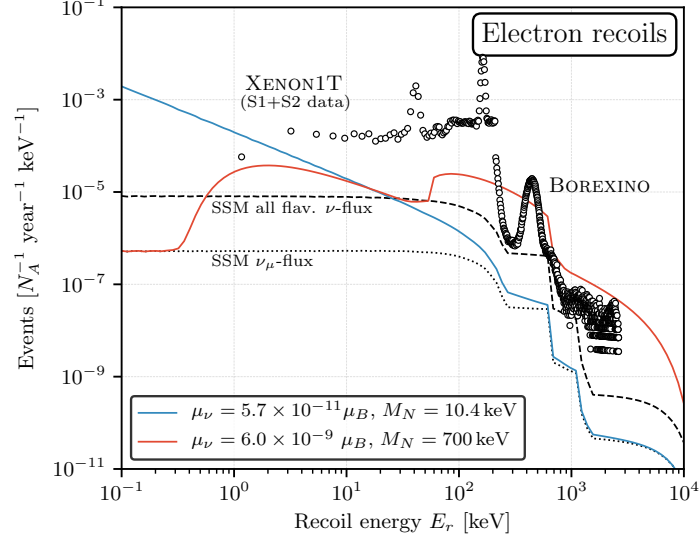


Figure 2 – Spectrum of neutrino-induced electron recoils for the Standard Solar Model (SSM, dotted and dashed black lines) and in two different scenarios with non-negligible neutrino magnetic moments (blue and red lines). We also compare to the data from Borexino [21] and Xenon1T [22].

mass  $M_N$ , while at higher  $M_N$ , Borexino takes over.

### 3 Astrophysical, Cosmological, and Accelerator Constraints

While direct dark matter searches are the most sensitive *terrestrial* probes of neutrino magnetic moments, astrophysical and cosmological constraints can be even stronger in large regions of parameter space.

#### 3.1 Stellar Cooling

In the hot plasma inside a star, the photon dispersion relation is modified in a way that can be interpreted as photons (or rather their in-medium counterparts called plasmons) acquiring a mass on the order of the plasma temperature  $T$ . Therefore, plasmon decays to  $\nu_L + N_R$ , mediated by the magnetic moment coupling, become possible if  $T \gtrsim M_N$ . Since neutrinos can leave the star unimpeded, this leads to significant energy losses [29, 30]. These losses modify stellar evolution and change, for instance, the mass of the helium core of red giant stars at the time of the helium flash. The latter, in turn, can be observed through the luminosity at the tip of the red giant branch in the Hertzsprung–Russell diagram [29, 31–33]. The resulting constraint, shown in purple in fig. 3, excludes neutrino magnetic moments down to  $\mu_\nu \sim \text{few} \times 10^{-12} \mu_B$  for light  $M_N$ , but peters out at  $M_N \gtrsim 10$  keV, the typical core temperature of a red giant star. The kink in the exclusion region is due to an additional energy loss process,  $\gamma + e^- \rightarrow \nu_L + N_R + e^-$ , which extends the sensitivity to somewhat larger  $M_N$ .

Note that stellar cooling constraints can be avoided in so-called “chameleon” models, in which  $M_N$  depends dynamically on the surrounding matter density.

#### 3.2 Supernova 1987A

The processes that lead to anomalous cooling of stars are also active in supernova cores, where they accelerate the cooling rate of the nascent neutron star [29, 34]. The latter is constrained by the observed duration of the neutrino burst from supernova 1987A, and the resulting constraint is delineated by the gray dashed line in fig. 3. Note the characteristic wedge shape of the

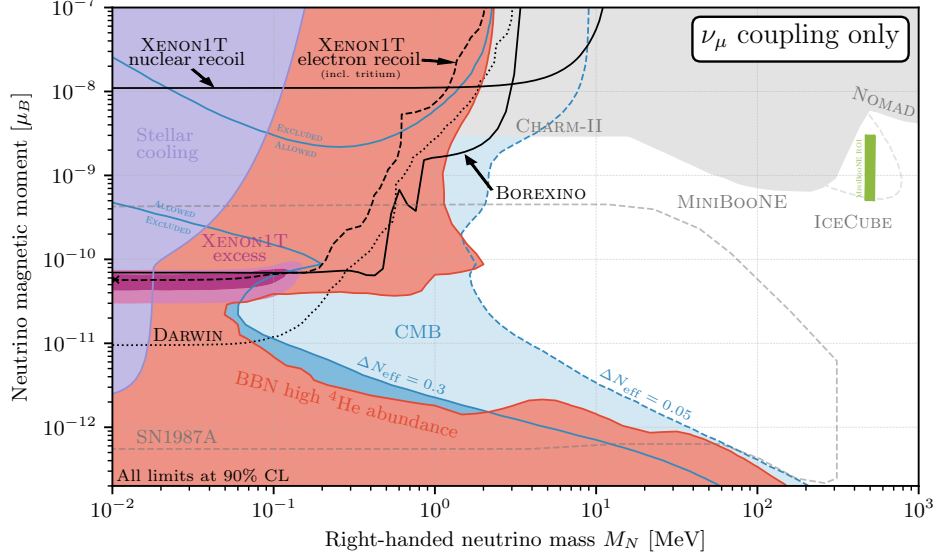


Figure 3 – Summary of constraints on neutrino magnetic moments as a function of the right-handed neutrino mass. We show limits from Xenon1T (dashed line and upper solid black line) and from Borexino (lower solid black line), as well as the expected sensitivity of DARWIN (dotted black). The Xenon1T electron recoil excess can be explained in the violet region at  $\mu_\nu \sim \text{few} \times 10^{-11} \mu_B$ . Stellar cooling excludes the region shown in purple, while SN 1987A is sensitive to the region delineated by the dashed gray line. Cosmology disfavors the red region via BBN, and the blue region through the  $N_{\text{eff}}$  measurement in the CMB. Fixed-target accelerator experiments exclude the upper gray regions. We finally show the region favored by some explanation attempts for the MiniBooNE anomaly (green), and the sensitivity of IceCube via double-bang signatures [28]. We comment in the text on the robustness of the various constraints.

excluded region, which is a reflection of the fact that for too large  $\mu_\nu$ , neutrinos will no longer be able to leave the supernova core without scattering and re-depositing their energy.

We remark that constraints from SN 1987A have recently been called into question by the authors of ref. [35], who argue that the observed neutrinos might not have originated from the cooling neutron star itself, but from the accretion flow surrounding it. In this case, they would carry no information on the cooling rate of the neutron star, and the limit would disappear.

### 3.3 Cosmology

For not too small  $\mu_\nu$ , the neutrino magnetic moment operator leads to the production of  $N_R$  in the early Universe. The presence of  $N_R$  has manifold consequences on the evolution of the Universe, especially during BBN:

- an increase in the energy density of relativistic species (measured through the parameter  $N_{\text{eff}}$ ) if  $M_N$  is below the BBN temperature,  $T_{\text{BBN}} \sim 1 \text{ MeV}$ . The resulting increased expansion rate implies that  $p \leftrightarrow n$  interactions freeze out faster and that neutrons have less time to decay. Both effects imply a larger abundance of heavy elements.
- a phase of full or partial matter domination around BBN if  $M_N \gg T_{\text{BBN}}$ , but the  $N_R$  lifetime is longer than a few minutes.
- a decrease in the baryon-to-photon ratio  $\eta$ . If  $N_R$  decays to photons and  $\nu_L$  happen after BBN, this decrease in  $\eta$  must be compensated by a larger  $\eta$  during BBN as  $\eta$  is measured very precisely in the CMB. The larger  $\eta$  during BBN renders deuterium disintegration less efficient and therefore production of heavy elements more efficient.
- a change in the photon-to-neutrino ratio at the CMB epoch (measured through  $N_{\text{eff}}$ ) if the  $N_R$  decay after neutrino decoupling.

Using a modified version of the AlterBBN code [36–38], we have simulated BBN in the presence of right-handed neutrinos and non-zero  $\mu_\nu$ . Comparing the predicted primordial abundances of light elements, especially  $^4\text{He}$ , with observations, we obtain the exclusion region shown in red in fig. 3. At  $M_N \lesssim \text{MeV}$ , or at low  $\mu_\nu$  and thus long  $N_R$  lifetime, the  $N_R$  are present during BBN, increasing the expansion rate of the Universe. Moreover, their eventual decay injects extra energy into the plasma after BBN. Note that there is a sweet spot at masses  $\lesssim \text{MeV}$  and  $\mu_\nu \sim 10^{-11} \mu_B$ , where the limit is relatively weak. There,  $N_R$  decouple around the QCD phase transition so that their abundance is significantly diluted by entropy production during the QCD phase transition, and at the same time their mass is sufficiently small to avoid a phase of full or partial matter domination.

However, when using the same simulation that predicts the  $^4\text{He}$  abundance to also predict the value of  $N_{\text{eff}}$  at recombination, we see that this sweet spot is closed. For instance, the parameter region favored by the Xenon1T excess is completely closed if the current limit  $\Delta N_{\text{eff}} < 0.05$  [39] is taken at face value. If we allow for larger  $\Delta N_{\text{eff}} \simeq 0.2$ , as suggested by the tension between primordial and late-time measurements of the Hubble constant, the Xenon1T region may still be marginally allowed.

Let us finally remark that cosmological limits are quite robust. Avoiding or relaxing them requires either a mechanism that prevents  $N_R$  production in the early Universe altogether, for instance by coupling  $N_R$  to a slowly rolling scalar field, such that the  $N_R$  mass in the early Universe is different from the one today. Or one could mitigate the problems created by  $N_R$  decay to  $\nu_L + \gamma$  by introducing a second decay mode to lighter SM singlets.

### 3.4 Accelerator Constraints

Coming back to Earth, an additional set of constraints on neutrino magnetic moments can be obtained from direct searches for  $N_R$  production in fixed-target accelerator experiments. Figure 3 shows in gray the limits derived from Charm-II, MiniBooNE, and NOMAD [40]. In the case of MiniBooNE, we also indicate in green the parameter region favored by certain attempts to explain the MiniBooNE anomaly [34, 41].

## 4 The Muon $g - 2$

We finally comment on the relation between neutrino magnetic moments and the anomalous magnetic moment of the muon,  $(g - 2)_\mu$ . We focus on the leptoquark scenario we have presented as an example in section 1. In the Lagrangian of the  $S_1$  leptoquark, the terms relevant to the generation of  $\mu_\nu$  through the diagram in fig. 1 (b) are

$$\mathcal{L}_{S_1} \supset y_1 \bar{b}_R^c N_R S_1 + y_2 \bar{Q}_L^3 L_L^i c S_1^\dagger + \text{h.c.} . \quad (2)$$

The second of these also generates loop contributions to  $(g - 2)_\mu$ , but naive dimensional analysis shows that these are smaller by about an order of magnitude than the observed discrepancy between theoretical predictions [42] and the BNL/Fermilab results [43, 44]. However, the  $S_1$  leptoquark contributes to the muon’s  $g - 2$  also through another interaction, namely the operator  $\mathcal{L} \supset y'_1 \bar{t}_R^c e_R^i S_1$ . This operator generates loops involving top quarks, and because having a top quark in the loop lifts the chiral suppression that normally plagues loop contributions to the muon  $g - 2$ , even a tiny coupling  $y'_1$  is sufficient to accommodate the experimental results.

## Acknowledgments

This work has been supported by the European Research Council (ERC) under the European Union’s Horizon 2020 research and innovation program (grant agreement No. 637506, “ $\nu$ Directions” and grant agreement No. 833280, “FLAY”). Fermilab is operated by the Fermi Research Alliance, LLC under contract No. DE-AC02-07CH11359 with the US DOE.

## References

- [1] V. Brdar, A. Greljo, J. Kopp, and T. Opferkuch, *JCAP* **01**, 039, (2021), [arXiv:2007.15563](#).
- [2] K. Fujikawa and R. Shrock, *Phys. Rev. Lett.* **45**, 963, (1980).
- [3] B. W. Lee and R. E. Shrock, *Phys. Rev. D* **16**, 1444, (1977).
- [4] S. T. Petcov, *Sov. J. Nucl. Phys.* **25**, 340, (1977), [*Yad. Fiz.*25,641(1977); Erratum: *Sov. J. Nucl. Phys.*25,698(1977); Erratum: *Yad. Fiz.*25,1336(1977)].
- [5] P. B. Pal and L. Wolfenstein, *Phys. Rev. D***25**, 766, (1982).
- [6] R. E. Shrock, *Nucl. Phys.* **B206**, 359–379, (1982).
- [7] M. Dvornikov and A. Studenikin, *Phys. Rev. D***69**, 073001, (2004), [hep-ph/0305206](#).
- [8] C. Giunti and A. Studenikin, *Rev. Mod. Phys.* **87**, 531, (2015), [arXiv:1403.6344](#).
- [9] J. P. Lees et al., *Phys. Rev. D***88**, no. 7, 072012, (2013), [arXiv:1303.0571](#).
- [10] M. Bauer and M. Neubert, *Phys. Rev. Lett.* **116**, no. 14, 141802, (2016), [arXiv:1511.01900](#).
- [11] S. Hirose et al., *Phys. Rev. Lett.* **118**, no. 21, 211801, (2017), [arXiv:1612.00529](#).
- [12] R. Aaij et al., *Phys. Rev. Lett.* **115**, no. 11, 111803, (2015), [arXiv:1506.08614](#), [Erratum: *Phys. Rev. Lett.*115,no.15,159901(2015)].
- [13] R. Aaij et al., *Phys. Rev. Lett.* **113**, 151601, (2014), [arXiv:1406.6482](#).
- [14] R. Aaij et al., *JHEP* **08**, 055, (2017), [arXiv:1705.05802](#).
- [15] R. Aaij et al., *Phys. Rev. Lett.* **111**, 191801, (2013), [arXiv:1308.1707](#).
- [16] R. Aaij et al., *JHEP* **02**, 104, (2016), [arXiv:1512.04442](#).
- [17] R. Aaij et al., *Phys. Rev. Lett.* **122**, no. 19, 191801, (2019), [arXiv:1903.09252](#).
- [18] D. Buttazzo, A. Greljo, G. Isidori, and D. Marzocca, *JHEP* **11**, 044, (2017), [arXiv:1706.07808](#).
- [19] I. Dorsner, S. Fajfer, and O. Sumensari, *JHEP* **06**, 089, (2020), [arXiv:1910.03877](#).
- [20] M. B. Voloshin, *Sov. J. Nucl. Phys.* **48**, 512, (1988), [*Yad. Fiz.*48,804(1988)].
- [21] M. Agostini et al., *Nature* **562**, no. 7728, 505–510, (2018).
- [22] E. Aprile et al., (2020), [arXiv:2006.09721](#).
- [23] A. Gutlein et al., *Astropart. Phys.* **34**, 90–96, (2010), [arXiv:1003.5530](#).
- [24] R. Harnik, J. Kopp, and P. A. N. Machado, *JCAP* **1207**, 026, (2012), [arXiv:1202.6073](#).
- [25] J. L. Feng et al., (2014), [arXiv:1401.6085](#).
- [26] K. S. Babu, S. Jana, and M. Lindner, (2020), [arXiv:2007.04291](#).
- [27] I. M. Shoemaker, Y.-D. Tsai, and J. Wyenberg, (2020), [arXiv:2007.05513](#).
- [28] P. Coloma, P. A. Machado, I. Martinez-Soler, and I. M. Shoemaker, *Phys. Rev. Lett.* **119**, no. 20, 201804, (2017), [arXiv:1707.08573](#).
- [29] G. G. Raffelt, *Stars as laboratories for fundamental physics*, 1996.
- [30] G. Raffelt, *Phys. Rept.* **320**, 319–327, (1999).
- [31] G. Raffelt and A. Weiss, *Phys. Rev. D* **51**, 1495–1498, (1995), [hep-ph/9410205](#).
- [32] S. Arceo-Díaz, K.-P. Schröder, K. Zuber, and D. Jack, *Astropart. Phys.* **70**, 1–11, (2015).
- [33] S. A. Díaz et al., (2019), [arXiv:1910.10568](#).
- [34] G. Magill, R. Plestid, M. Pospelov, and Y.-D. Tsai, *Phys. Rev. D***98**, no. 11, 115015, (2018), [arXiv:1803.03262](#).
- [35] N. Bar, K. Blum, and G. D’amico, *Phys. Rev. D***101**, 123025, (2020), [arXiv:1907.05020](#).
- [36] A. Arbey, *Comput. Phys. Commun.* **183**, 1822–1831, (2012), [arXiv:1106.1363](#).
- [37] A. Arbey, J. Auffinger, K. Hickerson, and E. Jenssen, *Comput. Phys. Commun.* **248**, 106982, (2020), [arXiv:1806.11095](#).
- [38] P. F. Depta, M. Hufnagel, and K. Schmidt-Hoberg, *JCAP* **05**, 009, (2020), [arXiv:2002.08370](#).
- [39] O. H. Philcox, M. M. Ivanov, M. Simonović, and M. Zaldarriaga, *JCAP* **05**, 032, (2020), [arXiv:2002.04035](#).
- [40] I. M. Shoemaker and J. Wyenberg, *Phys. Rev. D* **99**, no. 7, 075010, (2019), [arXiv:1811.12435](#).
- [41] S. N. Gninenko, *Phys. Rev. Lett.* **103**, 241802, (2009), [arXiv:0902.3802](#).
- [42] T. Aoyama et al., *Phys. Rept.* **887**, 1–166, (2020), [arXiv:2006.04822](#).
- [43] G. Bennett et al., *Phys. Rev. D* **73**, 072003, (2006), [hep-ex/0602035](#).
- [44] B. Abi et al., *Phys. Rev. Lett.* **126**, no. 14, 141801, (2021), [arXiv:2104.03281](#).